

**THERMOSONDE 2007:  
In-Situ Measurement of Optical Turbulence**

**E. A. Murphy  
P. Tracy  
R. R. Beland  
G. Y. Jumper  
K. Robinson  
G. Clement**

**7 May 2007**

**APPROVED FOR PUBLIC RELEASE; DISTRIBUTION UNLIMITED.**

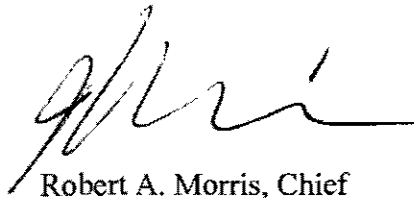


**AIR FORCE RESEARCH LABORATORY  
Space Vehicles Directorate  
29 Randolph Road  
AIR FORCE MATERIEL COMMAND  
Hanscom AFB, MA 01731-3010**

---

AFRL-VS-HA-TR-2007-1129

This technical report has been reviewed and is approved for publication.



Robert A. Morris, Chief  
Battlespace Environment Division



Edmund A. Murphy  
Author



Domenic F. Thompson, Maj, USAF, Chief  
Battlespace Surveillance Innovation Center

Using Government drawings, specifications, or other data included in this document for any purpose other than Government procurement does not in any way obligate the U.S. Government. The fact that the Government formulated or supplied the drawings, specifications, or other data does not license the holder or any other person or corporation; or convey any rights or permission to manufacture, use, or sell any patented invention that may relate to them.

This report is published in the interest of scientific and technical information exchange and its publication does not constitute the Government's approval or disapproval of its ideas or findings.

This report has been reviewed by the ESC Public Affairs Office (PA) and is releasable to the National Technical Information Service (NTIS).

Qualified requestors may obtain additional copies from the Defense Technical Information Center (DTIC). All other requestors should apply to the National Technical Information Service (NTIS).

If your address has changed, if you wish to be removed from the mailing list, or if the addressee is no longer employed by your organization, please notify AFRL/RVIM, 29 Randolph Rd., Hanscom AFB, MA 01731-3010. This will assist us in maintaining a current mailing list.

Do not return copies of this report unless contractual obligations or notices on a specific document require that it be returned.

**REPORT DOCUMENTATION PAGE**

Form Approved  
OMB No. 0704-01-0188

The public reporting burden for this collection of information is estimated to average 1 hour per response, including the time for reviewing instructions, searching existing data sources, gathering and maintaining the data needed, and completing and reviewing the collection of information. Send comments regarding this burden estimate or any other aspect of this collection of information, including suggestions for reducing the burden to Department of Defense, Washington Headquarters Services Directorate for Information Operations and Reports (0704-0188), 1215 Jefferson Davis Highway, Suite 1204, Arlington VA 22202-4302. Respondents should be aware that notwithstanding any other provision of law, no person shall be subject to any penalty for failing to comply with a collection of information if it does not display a currently valid OMB control number.

**PLEASE DO NOT RETURN YOUR FORM TO THE ABOVE ADDRESS.**

|  |             |                                     |                               |  |   |
|--|-------------|-------------------------------------|-------------------------------|--|---|
| 1. REPORT DATE (DD-MM-YYYY)<br>3 May 2007  |             | 2. REPORT TYPE<br>Scientific, Final |                               | 3. DATES COVERED (From - To)   |   |
| 4. TITLE AND SUBTITLE<br><br>THERMOSONDE 2007:<br>In-Situ Measurement of Optical Turbulence  |             |                                     |                               | 5a. CONTRACT NUMBER  |   |
|  |             |                                     |                               | 5b. GRANT NUMBER   |   |
|  |             |                                     |                               | 5c. PROGRAM ELEMENT NUMBER<br>61102F                                       |   |
| 6. AUTHORS<br>E.A. Murphy, P. Tracy, R.R. Beland, G.Y. Jumper, K. Robinson*,<br>and G. Clement*  |             |                                     |                               | 5d. PROJECT NUMBER<br>2304   |   |
|  |             |                                     |                               | 5e. TASK NUMBER<br>OT  |   |
|  |             |                                     |                               | 5f. WORK UNIT NUMBER<br>A1   |   |
| 7. PERFORMING ORGANIZATION NAME(S) AND ADDRESS(ES)<br><br>Air Force Research Laboratory /RVBYA<br>29 Randolph Road<br>Hanscom AFB, MA 01731-3010   |             |                                     |                               | 8. PERFORMING ORGANIZATION<br>REPORT NUMBER<br><br>AFRL-RV-HA-TR-2007-1129 |   |
| 9. SPONSORING/MONITORING AGENCY NAME(S) AND ADDRESS(ES)  |             |                                     |                               | 10. SPONSOR/MONITOR'S ACRONYM(S)<br>AFRL/RVBYA                             |   |
|  |             |                                     |                               | 11. SPONSOR/MONITOR'S REPORT<br>NUMBER(S)                                  |   |
| 12. DISTRIBUTION/AVAILABILITY STATEMENT<br>Approved for Public Release; distribution unlimited.  |             |                                     |                               |  |   |
| 13. SUPPLEMENTARY NOTES<br>*Stewart Radiance Laboratory, Utah State University Research Foundation, Bedford, MA 01730  |             |                                     |                               |  |   |
| 14. ABSTRACT<br><br>This report updates the 1982 Thermosonde technical report, by documenting the current configuration. The wires in the thermosonde are arranged as two legs of a Wheatstone bridge, which generates a voltage proportional to the resistance difference. The telemetry signal now consists of digital signal "counts," rather than analog frequency changes, the multiple segment calibration relationship has been replaced by a single straight line, and a new, lower signal calibration input point has been added to the calibration source. Synchronous detection of the telemetry signal has allowed the overall gain to be increased to approximately 600,000. Calibration voltages are read within 1mV for a range of voltages from the minimum, which is the noise floor of about 10 mV (equivalent to about 0.0005K up to a maximum output of 2.0 V. For a modest CT2 value of 0.0002K2M-2/3, the uncertainty in Cn2 is down to 1.5 percent. For a stronger CT2 of 0.001, overall Cn2 uncertainty is below 0.5% at low altitudes and starts to noticeably increase at 20 km, reaching a 4% uncertainty at 30 km due to pressure uncertainties. |             |                                     |                               |  |   |
| 15. SUBJECT TERMS<br>Temperature structure constant      Thermosonde      Turbulence measurement<br>Refractive index structure constant  |             |                                     |                               |  |   |
| 16. SECURITY CLASSIFICATION OF:  |             |                                     | 17. LIMITATION OF<br>ABSTRACT | 18. NUMBER<br>OF<br>PAGES<br>18  | 19a. NAME OF RESPONSIBLE PERSON           |
| a. REPORT  | b. ABSTRACT | c. THIS PAGE                        |                               |  | Edmund A. Murphy                          |
| UNCL   | UNCL        | UNCL                                | UNL                           |  | 19b. TELEPHONE NUMBER (Include area code) |

## Contents

|  |    |
|--|----|
| THERMOSONDE 2007: .....                                | 1  |
| In Situ Measurement of Optical Turbulence.....         | 1  |
| 1. Introduction.....                                   | 1  |
| 2. $C_n^2$ Measurement Principles.....                 | 1  |
| 3. Description of the Instrument .....                 | 2  |
| 4. Calibration.....                                    | 5  |
| 4.1 Telemetry Calibration.....                         | 5  |
| 4.2 Instrument Noise.....                              | 6  |
| 4.3 Calibration Theory .....                           | 7  |
| 4.4 Calibration Procedure .....                        | 8  |
| 4.5 Calibration Example .....                          | 9  |
| 4.6 End to End Check of the System .....               | 10 |
| 4.7 Universal Calibration Curve Fits .....             | 11 |
| 4.8 Uncertainty due to the Universal Calibration ..... | 12 |
| 5. Instrumentation Errors .....                        | 14 |
| 5.1 Pressure and Mean Temperature.....                 | 14 |
| 5.2 Temperature Fluctuation.....                       | 15 |
| 5.2.1 Accuracy .....                                   | 15 |
| 5.2.2 Precision.....                                   | 16 |
| 5.2.3 Universal Calibration Curve .....                | 16 |
| 5.2.4 Noise Floor.....                                 | 16 |
| 5.3 Effect of the Above Errors.....                    | 16 |

|   |    |
|---|----|
| 5.4 Other Instrument Related Factors: .....   | 17 |
| 5.4.1 Heat Transfer – Altitude Limits .....   | 17 |
| 5.4.2 RMS Chip .....                          | 17 |
| 5.4.3 Telemetry system .....                  | 17 |
| 5.4.4 Environmental Factors .....             | 17 |
| 5.4.5 Balloon Wake .....                      | 17 |
| 5.4.6 Stationarity – Homogeneity Issues ..... | 18 |
| 6. Summary .....                              | 18 |
| REFERENCES .....                              | 19 |

## Illustrations

|   |    |
|---|----|
| Figure 1. Two views of the thermosonde showing probes, beam and radiosonde. ....  | 3  |
| Figure 2. Functional schematic of the thermosonde integrated with the VIZ radiosonde.   | 3  |
| Figure 3. A graphical representation of the thermosonde electronics in ACSL simulation.<br>.....  | 4  |
| Figure 4. The probe calibration box is used to simulate the probes as described in Section 4.5. As the $\Delta R$ is switched over its widest range, the RMS voltage output from the signal conditioning electronics is compared to the RMS voltage obtained through the whole system as would be in an actual flight. ....         | 11 |
| Figure 5. Calibration points from 16 thermosonde boards plotted with universal calibration curve.....   | 12 |
| Figure 6. Difference between universal calibration curve and calibration points expressed as Temperature difference assuming a nominal resistance value of $27\Omega$ .....   | 14 |
| Figure 7. Error between universal curve and calibration points, as percent of the temperature difference. The mean error at any input temperature is shown as connected squares. Finally, the standard deviation of the calibration from the curve fit is shown as the line which remains in the positive portion of the graph..... | 15 |

## Tables

|   |    |
|---|----|
| Table 1. Calibration sheet for thermosonde board 256, which is a typical example. ....                    | 10 |
| Table 2. Comparison of voltage from board to voltage from the data reduction program.<br>.....            | 10 |
| Table 3. Comparison of the universal calibration curve to the calibration values from the 16 boards. .... | 13 |

## 1. INTRODUCTION

The purpose of this report is to describe the thermosonde instrument used to obtain the vertical profile of the refractive index structure constant,  $C_n^2$ . The balloon-borne thermosonde instrument is a package originally developed by NASA, then improved over the years by the Air Force Geophysics Laboratory, now AFRL/VSBL. The instrument has evolved through the years, but basically it involves measurements of the temperature difference across a fixed horizontal distance, typically 1m. This is done while the balloon ascends at an approximately constant vertical velocity, 5 m/s. This temperature difference is used to obtain the temperature structure constant,  $C_T^2$ . The refractive index structure constant,  $C_n^2$  is obtained from  $C_T^2$  by using of the Dale-Gladstone equation.

In the years since the last thermosonde technical report<sup>1</sup> in 1982, calibration procedures have gone through several changes. The evolution began with a change in radiosonde telemetry method from analog frequency changes to digital “counts”. Lower instrument noise has allowed the dual gain calibration curves to be replaced by a single gain calibration curve. The multiple segment calibration relationship was replaced by a single straight line. A new, lower signal calibration input point has been added to the calibration source. As instrument noise has reduced and component and assembly quality has improved, individual instrument calibration curves have been replaced by a single universal calibration curve. The approach to handling instrumentation noise has also changed.

The purpose of this report is to document the current thermosonde configuration. An important section is a description of the current calibration methodology and the new universal calibration curve. Also documented are the uncertainties associated with the current hardware and new calibration procedures.

## 2. $C_N^2$ MEASUREMENT PRINCIPLES

The basis for the thermosonde measurement is the analysis of random processes. To the extent that the fluctuations of a variable,  $Y$ , in the atmosphere can be considered a homogeneous and isotropic random process, one can pass two sensors through the atmosphere a distance,  $r$ , apart and generate the structure function,  $D_Y(r)$  where<sup>2</sup>

$$D_Y(r) = \left\langle [Y(x) - Y(x+r)]^2 \right\rangle. \quad (1)$$

A. N. Kolmogorov<sup>3</sup> postulated that for velocity fluctuations in a fully developed turbulent flow, the velocity structure function,  $D_v(r)$ , would have the following equivalent relation to the distance in the structure function:

$$D_v(r) = C_v^2 r^{2/3} \quad (2)$$

where the constant  $C_v^2$  is known as the velocity structure constant. If one were to observe the velocity power spectral density,  $S_{rr}(K)$ , it would have the equivalent relation:

$$S_{rr}(K) = 0.25 C_v^2 K^{-5/3} \quad (3)$$

where  $K$  is the wave number of the eddies.

The random turbulence field was assumed to be locally homogeneous and isotropic for scales less than the largest eddies, which are the turbulent kinetic energy source (the outer scale,  $L_0$ ), but larger than the smallest eddies, which are the sizes of the viscous energy dissipation (the inner scale,  $l_0$ ). The range between the scales, where the turbulent kinetic energy is passed down from the larger eddies to the smaller by inertial processes, is known as the inertial range. While the condition of inertial range “equilibrium turbulence” defined above is not always present in the atmosphere, functional relationships with a power near  $2/3$  are surprisingly prevalent.

Corrsin<sup>4</sup>, Yaglom, and Obukhov<sup>5,2</sup> independently extended the Kolmogorov theory to passive scalars, and showed that the structure function of conservative passive scalars, such as temperature and refractive index, should also follow the  $2/3$  power law (Eq. 2).

In this report, it is the refractive index structure constant,  $C_n^2$ , that is of interest. It is obtained from the temperature structure constant,  $C_T^2$ , via the Dale-Gladstone relation, i.e.,

$$C_n^2 = \left( 79 \times 10^{-6} \frac{P}{T^2} \right)^2 C_T^2. \quad (5)$$

In the above expression,  $P$  is the atmospheric pressure in millibars and  $T$  is the temperature in degrees Kelvin.

### 3. DESCRIPTION OF THE INSTRUMENT

The fine resistance wires used in the thermosonde have a time constant less than 2 ms at sea level. This permits the measurement of rapidly varying temperature fluctuations. Low constant current passes through the wires, which operate as low-overheat resistance wire detectors. The two resistance probes are legs of a Wheatstone bridge, which generates a voltage proportional to the resistance difference. The

instrumentation must be sensitive enough to detect temperature differences in milli-degrees, Kelvin. The fluctuating difference voltage is amplified, filtered, and passed to an onboard analog processor that computes the root mean square (RMS) of the fluctuating temperature difference. The time constant of the RMS chip is set to 3.7s. The thermosonde instrument is attached to a standard meteorological radiosonde measuring the ambient temperature, pressure, humidity (Figure 1). The RMS chip output is sampled every 1 to 2 seconds (depending on the type of radiosonde) by a spare channel of the radiosonde and relayed to the ground with the meteorological data. The radiosonde also uses either GPS or the Loran navigation system, from which position and wind velocity are determined and relayed down to the ground station. The ground station has special software to extract the spare channel data. A functional schematic of the thermosonde system is shown in Figure 2.

In order to understand the response of the thermosonde, an engineering model was assembled and analyzed in a computer simulation. The basis of the engineering model are two AFGL technical reports<sup>1,6</sup>, the NASA technical note by the thermosonde developer, Jack Bufton<sup>7</sup>, and recent inhouse engineering work<sup>8</sup>. The simulation model uses the software package, Advanced Continuous Simulation Language (ACSL)<sup>9</sup>. A graphical model of the system is shown in Figure 3.

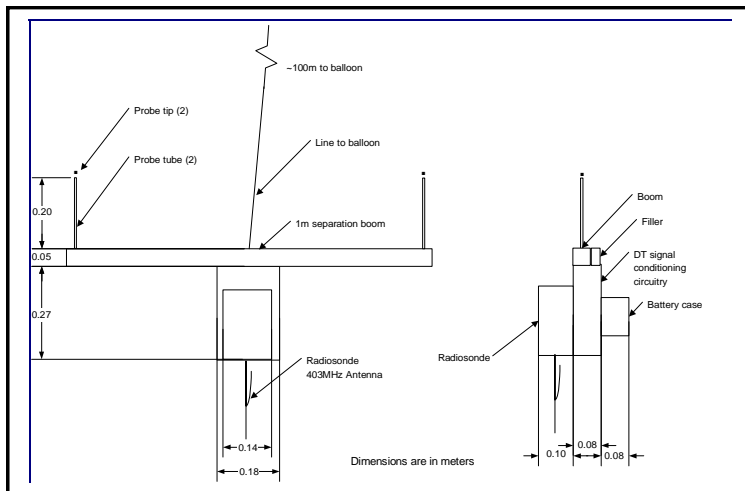


Figure 1. Two views of the thermosonde showing probes, beam and radiosonde.

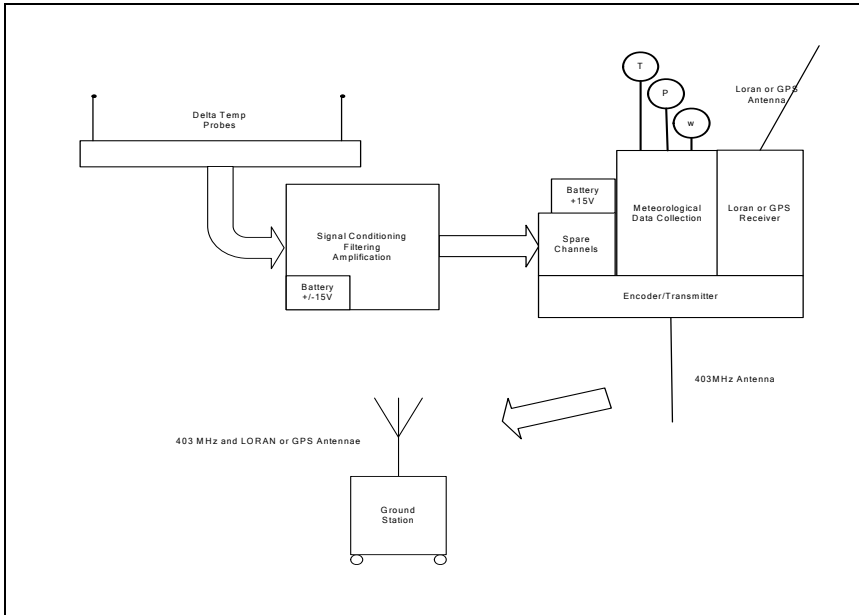


Figure 2. Functional Schematic of the thermosonde integrated with the VIZ radiosonde

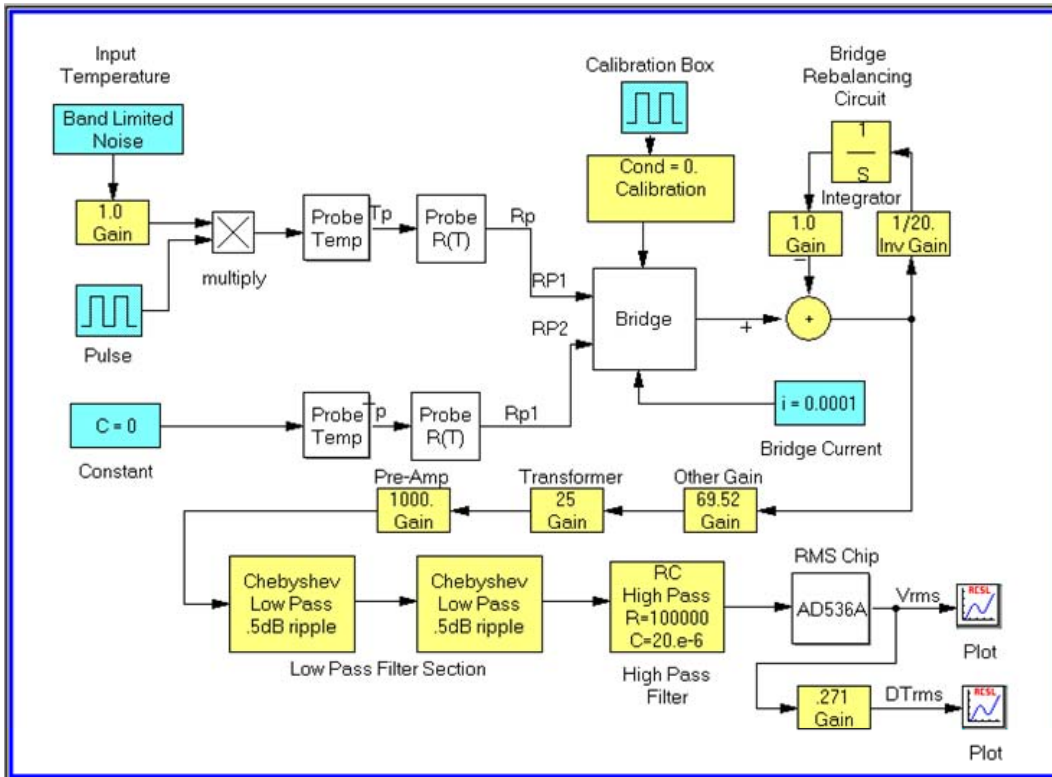


Figure 2. A graphical representation of the thermosonde electronics in ACSL simulation.

Referring to the graphical representation in Figure 3, there are some other technical details that give a more complete description of the instrument. The calibration box is attached to the bridge, in place of the probes, using a procedure described below.

Since there can be some drift of resistance difference as the instrument changes temperature as it is ascending through the atmosphere, there is a bridge rebalancing circuit with a time constant of 20s.

The overall gain of the instrument is approximately 600,000, which is possible due to an aspect of the circuit that is not part of the simulation, synchronous detection. The bridge and the initial part of the circuit, is actually powered by alternating current at 3kHz. The desired signal is amplitude modulated on this 3kHz signal. After most of the amplification, a synchronous detector strips out the correct frequency.

After low and high pass filtering, the signal is passed to a root-mean-square integrated circuit or “RMS Chip”. This does not perform an exact mathematical equivalent of the RMS operation. Whereas the chip is often represented by a first order integrator with a fixed time constant, the circuit actually gives different time constants for the rise and fall of the input signal<sup>8</sup>. The output of the RMS chip is sampled and passed to the radiosonde for transmission to the ground station.

## **4. CALIBRATION**

This section documents the current calibration process used for thermosondes

### **4.1 Telemetry Calibration**

The initial calibration transformation is from received digital counts to RMS voltage. Two brands of radiosondes have been used through the period, VIZ (now Lockheed Martin – Sippican) and Väisälä. The VIZ sondes were individually calibrated prior to flight, and have been found to have very little variation from sonde to sonde.

The Väisälä sondes have individual calibration constants for the interface box through which the thermosonde electronics are connected to the radiosonde. There can be large variations from box to box. The calibrations are checked periodically and found to be accurate. The calibration constants are part of the input into the data reduction program.

## 4.2 Instrument Noise

When calibrating the thermosonde instrument, one setting is an open circuit, which equates to a zero input signal. With this input, there is an output voltage from the system, which is interpreted as the instrument noise floor. In the laboratory, this noise floor is 0.019 to 0.025 Volts. When the zero-signal input to the RMS chip was sampled in the laboratory, it was found to be a Gaussian distribution with a mean of 0 and a standard deviation of approximately the output noise floor of the chip. After the instrument is released, and ascending through the atmosphere behind a balloon, the minimum voltage is usually a few mV lower than the noise floor observed in the laboratory. This is not considered unusual since electronic noise is higher inside buildings due to light bulbs and other electrical appliances and instruments. The apparent flight noise floor is often not constant, but may slowly drift lower or higher as the flight progresses. A representative value of the inflight noise is recorded and entered into the data reduction program.

The current method of handling instrument noise is to assume that the noise is independent of input signal and uncorrelated with that signal, and that the noise amplitude is only slowly varying with environmental conditions. The signal into the RMS chip is then:

$$V_i = V_s + V_n \quad (6)$$

Where the subscripts represent input, signal, and noise respectively. The output of the RMS chip,  $V_{rms}$ , can be represented by the following equation:

$$V_{rms} = \left[ \frac{1}{\tau} \int_0^{\tau} (V_s + V_n)^2 dt \right]^{1/2} \quad (7)$$

where  $\tau$  is the time constant of the RMS chip which is long compared to the fluctuations of the turbulent signal and the noise. Performing the square, and recognizing that the integral is the time average of the quantity over  $\tau$ , we obtain the result:

$$V_{rms}^2 = \langle V_s^2 \rangle + 2 \langle V_s V_n \rangle + \langle V_n^2 \rangle \quad (8)$$

where the brackets indicate the time average. Before entering the RMS chip, the noise is equally distributed in the positive and negative direction. In addition, the bridge balancing circuit insures that the input signal is also balanced about a mean of zero volts, to within the time constant of the balancing circuit ( $\sim 20$ s). Further, we assume that there is no correlation between signal and noise. The result is that the middle, cross product term averages out to nearly zero, leaving us with the equation:

$$V_{rms}^2 = \langle V_s^2 \rangle + \langle V_n^2 \rangle \quad (9)$$

When the input signal is zero, there is a small output from the chip. This is interpreted as the noise. The RMS chip has converted the oscillating circuit noise to a positive value, which is averaged over time, and, in fact, does not vary significantly over a reasonable period of observation on the bench. Since we are interested in the amplified signal from the bridge,  $V_s$ , the RMS chip output voltage is always corrected for the noise. In calibration, the noise is determined when no resistance change is introduced from the calibration box, and each subsequent calibration output is corrected using the formula:

$$V_s = \sqrt{V_{rms}^2 - V_n^2} \quad (10)$$

Where we have dropped the time average brackets, and each voltage is assumed to be a time averaged value. This procedure is consistent with guidance in correcting for noise in AC voltmeters<sup>11</sup>. This correction is insignificant for higher values of signal, but becomes significant as the signal strength decays to low values.

### 4.3 Calibration Theory

It is assumed that the change in resistance of a material with a change in temperature is nearly linear, and for modest temperature differences, it can be expressed as:

$$R(T) = R_0 [1 + \alpha(T - T_0)] \quad (11)$$

where the subscript,  $_0$ , denotes a reference temperature, usually chosen to be 0°C. Where  $\alpha$  is the temperature coefficient of resistivity, and it has a value of  $0.00375\text{K}^{-1}$  for the thermosonde probe wire.

In the thermosonde, the Wheatstone bridge detects a difference in resistance between the two probe circuits. Whereas, there are resistance differences in the parts of the circuit other than the thin wire sensors, there is a bridge balancing circuit that automatically balances slow changes in the resistance (time constant  $\sim 20\text{s}$ ), and the amplifier filters out changes that are slower than the expected turbulence. Therefore it is the difference in resistance of the two fine wire sensors that is actually analyzed. The difference in resistance in the two sensors is then:

$$\begin{aligned} \Delta R &= R_1(T_1) - R_2(T_2) \\ &= R_{01} + \alpha R_{01}(T_1 - T_0) - R_{02} - \alpha R_{02}(T_2 - T_0) \end{aligned} \quad (12)$$

Further, define:

$$R_0 = \frac{1}{2}(R_{01} + R_{02})$$

$$\delta = R_{01} - R_{02}$$

Substituting the definitions into Equation (7) and rearranging, we obtain:

$$\Delta R = \alpha R_0 (T_1 - T_2) + \delta \left[ 1 + \frac{\alpha}{2} (T_1 + T_2 - 2T_0) \right] \quad (13)$$

In practice, the reference temperature should not be too different from the measurement temperatures, consistent with the linear approximation, and  $\alpha$  is a small number, so the term in brackets is usually not much larger than 1. If the probe pairs are chosen to have nearly identical resistances such that  $\delta \ll R_0$  then the final working equation is:

$$\Delta R = \alpha R_0 \Delta T \quad (14)$$

where  $\Delta T$  is the difference in the temperature of the two probe sensors, which is the basis for the structure function calculation that defines the turbulence level.

#### 4.4 Calibration Procedure

The Wheatstone Bridge of the thermosonde is driven with a small AC current alternating at 3kHz. The wires operate in low overheat ratio mode, or as cold wire probes. Because of the dynamic bridge rebalancing and the need to reduce noise, the thermosonde circuit includes a passband filter to eliminate DC and high frequency noise from the turbulence signal: The bandwidth is determined by a 4 pole Butterworth and low pass filter network whose 3dB frequencies are 1kHz and 0.2Hz respectively. The turbulence signal in this passband is suitably amplified and finally passed through an RMS module with a nominal time constant of 3.75s. The RMS voltage is the thermosonde output that is fed into the radiosonde telemetry system.

As a result of Equation 9, above, a linear relation is expected between the input  $\Delta T$  and the output  $V_{rms}$ ; however, this is not assumed. Since the board filters out all but the narrow turbulence and, a special calibration instrument was designed and fabricated that switches known resistors in and out of the Wheatstone bridge, in place of the wire probes. The two probe wires are brought into the box and connected to two nearly identical resistors of  $27\Omega$  each. One of those resistors is part of a parallel circuit that is designed to allow one or more other known resistors to be switched in and out of the circuit at 20Hz. In other words, one probe circuit alternates between a resistance  $27\Omega$  and a lower resistance based

on the value of the switched in resistor. The calibration box effectively provides a square wave input of resistance difference to one leg of the bridge, varying between 0 and a specified resistance value,  $\Delta R$ . The bridge balancing circuit balances the two sides so that this square wave becomes symmetrically positioned about 0 volts.

The nominal temperature disturbances are assumed to be either sinusoidal or linear combinations of sinusoidal disturbances. Since root mean square of a square wave is twice that of a sine wave, the resistance is halved to give the equivalent of a sinusoidal disturbance. Hence, for the calibration process, the temperature difference, input calibration resistance difference relationship is determined by the formula:

$$\Delta T_{cal} = \frac{\Delta R_{cal}}{2\alpha R_0} \quad (15)$$

Each board is calibrated by measuring the voltage of the output of the RMS chip on the board for a progression of input resistance differences. Note that while  $\alpha$  is a property of the probe wire material,  $R_0$  can vary since it is also a function of probe wire geometry. Even though the calibration board has nominal resistance ( $R_0$ ) of  $27\Omega$ , each probe pair will have an  $R_0$  that is the mean of the reference resistance of each probe pair, and will vary about  $27\Omega$ . Therefore, the  $\Delta T \cdot R_0$  product is recorded, which is  $\Delta R_{cal} / 2\alpha$ .

## 4.5 Calibration Example

The calibration procedure begins by attaching the leads that would normally go to the probes to the calibration box inputs. After checking to insure proper input current to the bridge, a DC Voltmeter is attached to the output of the RMS chip, and the calibration box is set to the maximum  $\Delta R$  value of  $0.052234\Omega$ . The gain of the amplifier on the thermosonde board is set to produce an output of  $1.950V$  out of the RMS chip. Next  $\Delta R$  is set to 0, and the board is allowed to settle to the noise floor, typically around  $0.02V$ , which is recorded. An example of a typical calibration sheet is shown in Table 1. Column 1 is the input  $\Delta R$ ; column 4 is the output voltage from the RMS chip. The input resistance is set for each of the remaining values of  $\Delta R$  and the voltages are recorded. Also shown in the table are some ancillary calculations: Column 2 shows the input  $\Delta R$  divided by  $2\alpha$ , column 2 is the equivalent  $\Delta T$  for the nominal  $R_0$  of  $27\Omega$ . Finally, the last column is the voltage output after the noise correction, Equation 5, for each input resistance value.

| DELTA R  | Delta R/2alpha | delT     | Board 265 | 265 COR |
|----------|----------------|----------|-----------|---------|
| 0        |                |          | 0.021     | 0.000   |
| 0.001042 | 0.138933       | 0.005069 | 0.046     | 0.041   |
| 0.003137 | 0.418239       | 0.015259 | 0.121     | 0.119   |
| 0.005215 | 0.695330       | 0.025368 | 0.196     | 0.195   |
| 0.010445 | 1.392715       | 0.050810 | 0.392     | 0.391   |
| 0.015676 | 2.090128       | 0.076254 | 0.586     | 0.586   |
| 0.020894 | 2.785918       | 0.101639 | 0.785     | 0.785   |
| 0.025670 | 3.422729       | 0.124872 | 0.964     | 0.964   |
| 0.031088 | 4.145021       | 0.151223 | 1.166     | 1.166   |
| 0.036600 | 4.880032       | 0.178038 | 1.372     | 1.372   |
| 0.041801 | 5.573507       | 0.203338 | 1.563     | 1.563   |
| 0.047018 | 6.269031       | 0.228713 | 1.757     | 1.757   |
| 0.052234 | 6.964583       | 0.254089 | 1.950     | 1.950   |

Table 1. Calibration sheet for thermosonde board 256, which is a typical example.

#### 4.6 End to End Check of the System

The above calibration procedure insures that the temperature difference sensed by the resistance wires is properly converted to volts at the output of the RMS chip. This is only the first of the several operations performed by the thermosonde system before data is output to the user. The entire process is shown in Figure 4. In calibration, the thermosonde signal processing board is checked for volts. When fully assembled, that voltage is sent to the radiosonde interface and analog-to-digital unit. The digital unit converts volts to counts and sends the signal into the radiosonde where it is send down to the ground station as spare channel information with the regular meteorological information. That signal is sent on a 403MHz carrier to the receiver of the Ground Station. The received temperature difference data is processed then output as counts. The counts are then converted back to voltage by post-processing software, and then further converted to temperature difference. These conversions from volts to counts to radio signal then back again involve two conversion factors which are unique to each interface unit and radiosonde. An end to end check of the system was performed in the laboratory where the voltage output from the thermosonde board was compared to the voltage output from the data reduction software. The results, shown in Table 2, are quite encouraging, in that quantities are either identical, or differ by 1 or 2 in the 4<sup>th</sup> significant figure.

|                 |       |       |       |       |       |       |       |
|-----------------|-------|-------|-------|-------|-------|-------|-------|
| Volts Out       | 1.154 | 1.389 | 1.187 | 0.967 | 0.787 | 0.586 | 0.197 |
| Counts to Volts | 1.153 | 1.391 | 1.186 | 0.967 | 0.787 | 0.586 | 0.197 |

Table 2. Comparison of voltage from board to voltage from the data reduction program.

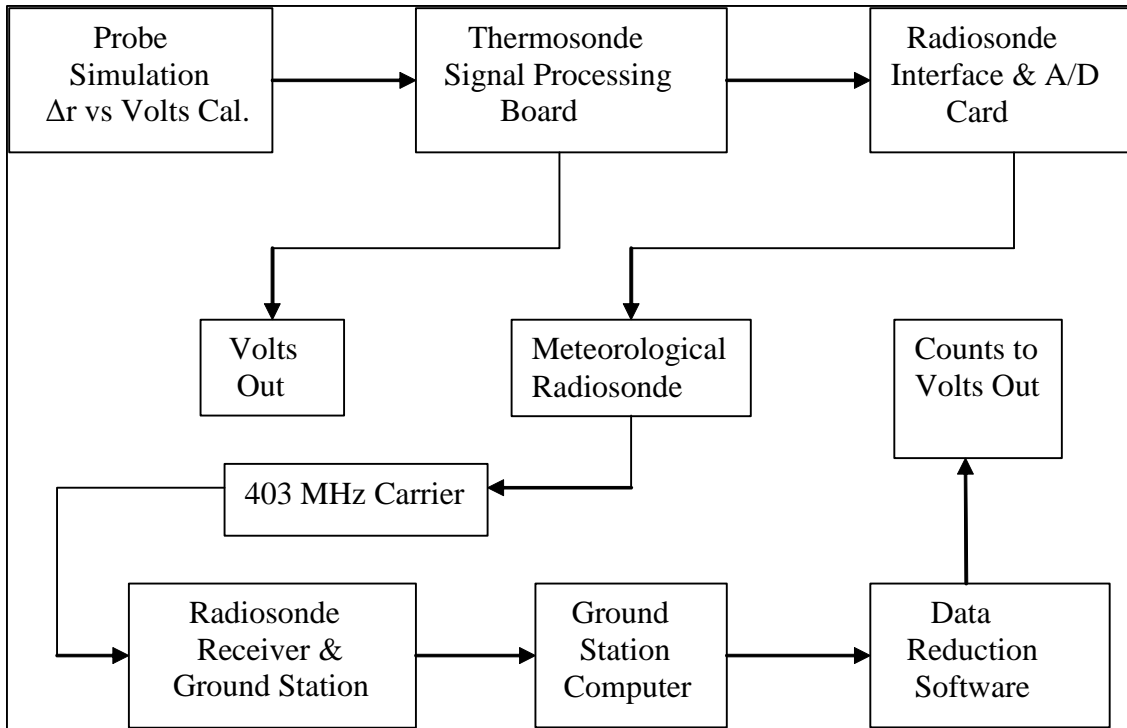


Figure 3. The probe calibration box is used to simulate the probes as described in Section 4.5. As the  $\Delta R$  is switched over its widest range, the RMS voltage output from the signal conditioning electronics is compared to the RMS voltage obtained through the whole system as would be in an actual flight.

## 4.7 Universal Calibration Curve Fits

With improved quality control of thermosonde parts and assembly, it was observed that after adjusting the gain of a board at the highest calibration setting, the output voltage at intermediate settings appeared to be very reproducible. Following the calibration analysis reported in this section, it was determined that a single (universal) calibration curve could be used for the thermosondes. The single universal calibration curve was the result of the calibration of 16 thermosonde boards.

As described in section 4.2, the new procedure assumes that the input to the RMS chip is composed of signal and noise. With this assumption, the output of the RMS chip is always corrected by Equation 5 to obtain the signal. For historical reasons the voltage signal may – or may not be referred to as  $V_{rms}$ . The calibration curve is applied to the signal voltage after correction for noise. This technique has the advantage of insuring that all the corrected calibration curves run through the origin. The data from the calibration of 16 boards are shown in Figure 4. The equivalent  $R_0 \Delta T$  is on the ordinate; the corrected (signal input) RMS voltage is on the abscissa. A straight-line calibration curve fits the data quite well. The universal calibration formula is:

$$R_0 \Delta T = 3.572 \Delta V_{in} \quad (16)$$

As shown on the curve, this correlation has a correlation coefficient, R, of 1, which is the result of rounding up the value: 0.999969.

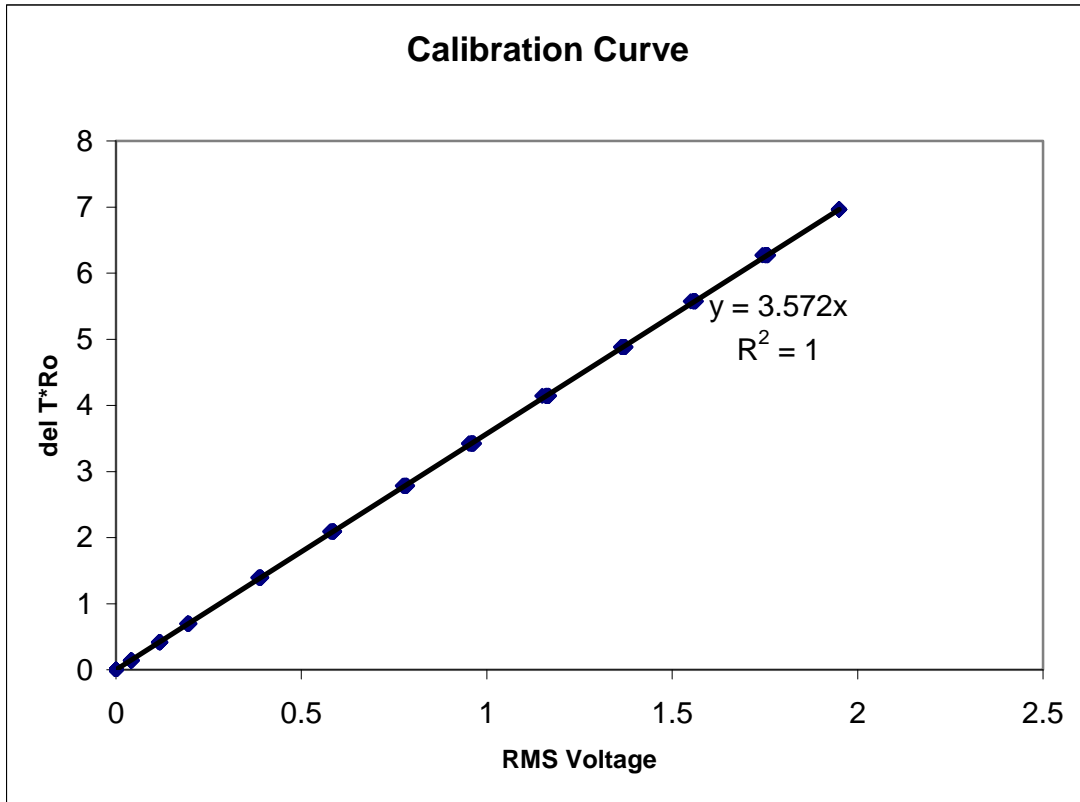


Figure 4. Calibration points from 16 thermosonde boards plotted with universal calibration curve.

#### 4.8 Uncertainty due to the Universal Calibration

After achieving the above curve fit, uncertainty estimates were made by comparing the fit to each of the 16 calibration points for each Delta T\*R<sub>0</sub> level. For each level, the uncertainty, as defined as the variance of the differences from the calibration curve and the actual points, was computed. For purposes of comparison, a nominal value of R<sub>0</sub> equal to 27Ω is used to depict the error in terms of temperature uncertainty. The results of the calculations are shown in Table 1. A plot of the difference between calibration curve and calibration points for 16 boards is shown in Figure 6. The maximum errors are less than 10% of the measured value, which occurs at the lower temperature value, as shown in

Figure 7. For a temperature difference of 0.015K, the maximum error is around 2% or less, with mean errors less than a percent. The standard deviation of the fit from the calibration points was used as the uncertainty, which has a maximum of ~6% at the lowest temperature, and decreases 1.5% at 0.015K, to well below a percent as temperature increases.

| Del T*Ro | Del T (K) | Avg Err   | %Err   | Var (K)  | St Dev of Fit | St Dev (%) | Var of Fit |
|----------|-----------|-----------|--------|----------|---------------|------------|------------|
| 0        | 0         | 0         | 0.00%  | 0        | 0.00E+00      | 0.00%      | 0.00E+00   |
| 0.138933 | 0.005146  | -0.000284 | -5.52% | 3.92E-07 | 3.17E-04      | 6.16%      | 1.01E-07   |
| 0.418239 | 0.01549   | -0.00011  | -0.71% | 6.59E-07 | 1.93E-04      | 1.25%      | 3.74E-08   |
| 0.69533  | 0.025753  | 3.57E-05  | 0.14%  | 1.15E-06 | 2.10E-04      | 0.81%      | 4.40E-08   |
| 1.392715 | 0.051582  | 0.000197  | 0.38%  | 2.82E-06 | 3.82E-04      | 0.74%      | 1.46E-07   |
| 2.090128 | 0.077412  | 0.000139  | 0.18%  | 5.04E-06 | 4.55E-04      | 0.59%      | 2.07E-07   |
| 2.785918 | 0.103182  | -1.92E-06 | 0.00%  | 6.04E-06 | 4.73E-04      | 0.46%      | 2.24E-07   |
| 3.422729 | 0.126768  | -0.000165 | -0.13% | 8.27E-06 | 5.79E-04      | 0.46%      | 3.35E-07   |
| 4.145021 | 0.153519  | -0.000244 | -0.16% | 9.9E-06  | 6.56E-04      | 0.43%      | 4.30E-07   |
| 4.880032 | 0.180742  | -0.000345 | -0.19% | 5.99E-06 | 5.91E-04      | 0.33%      | 3.49E-07   |
| 5.573507 | 0.206426  | 0.000192  | 0.09%  | 6.36E-06 | 5.30E-04      | 0.23%      | 2.81E-07   |
| 6.269031 | 0.232186  | 0.000331  | 0.14%  | 9.56E-06 | 6.93E-04      | 0.30%      | 4.80E-07   |
| 6.964583 | 0.257948  | -1.14E-05 | 0.00%  | 1.78E-10 | 1.21E-05      | 0.00%      | 1.46E-10   |

Table 3. Comparison of the universal calibration curve to the calibration values from the 16 boards.

As a result of the new universal calibration curve, the calibration procedure now consists of setting the highest voltage and checking intermediate levels to insure that the boards conform to past standards and that the universal curve is applicable.

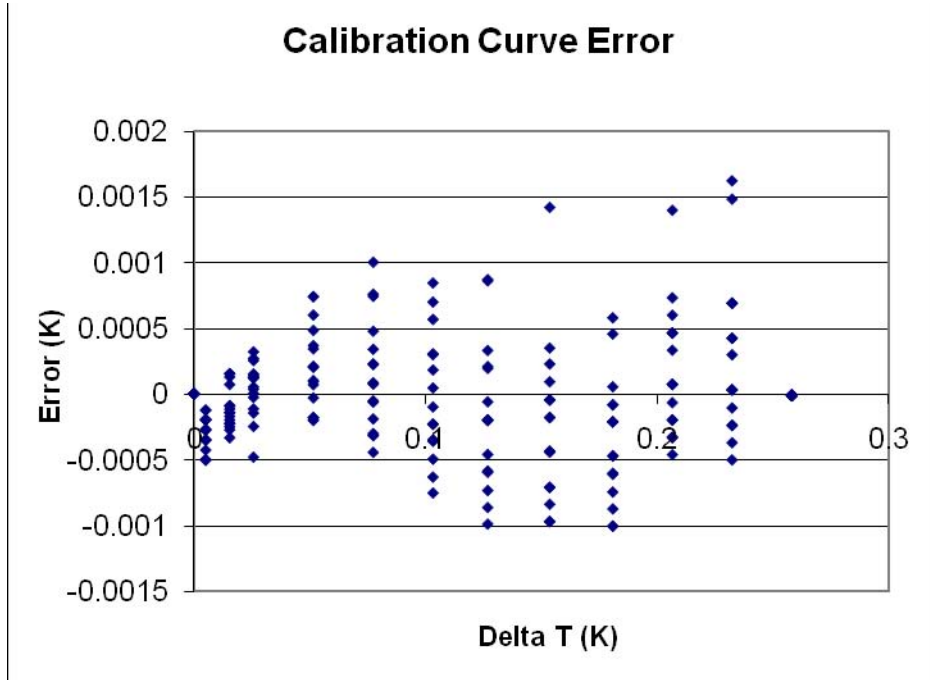


Figure 5. Difference between universal calibration curve and calibration points expressed as Temperature difference assuming a nominal resistance value of  $27\Omega$ .

## 5. INSTRUMENTATION ERRORS

The thermosonde instrument is composed of standard meteorological radiosonde components and the probes temperature fluctuation conditioning circuit. Instrumentation errors in optical turbulence measurements can be attributed to errors in the temperature and pressure sensors of the radiosonde, and temperature fluctuation errors in the thermosonde measurements.

### 5.1 Pressure and Mean Temperature

The pressure sensors of current radiosondes have an accuracy of 0.5 mbar, which is 0.05% of sea level pressure to 5% at maximum altitude. The temperature sensor has an accuracy of 0.2K at sea level, which degrades to 0.4K at maximum altitude. This is, at worst 0.2% of the ambient temperature throughout the range<sup>10</sup>. Systematic errors are minimized by calibration of the pressure sensor of each radiosonde against a high precision barometer at launch.

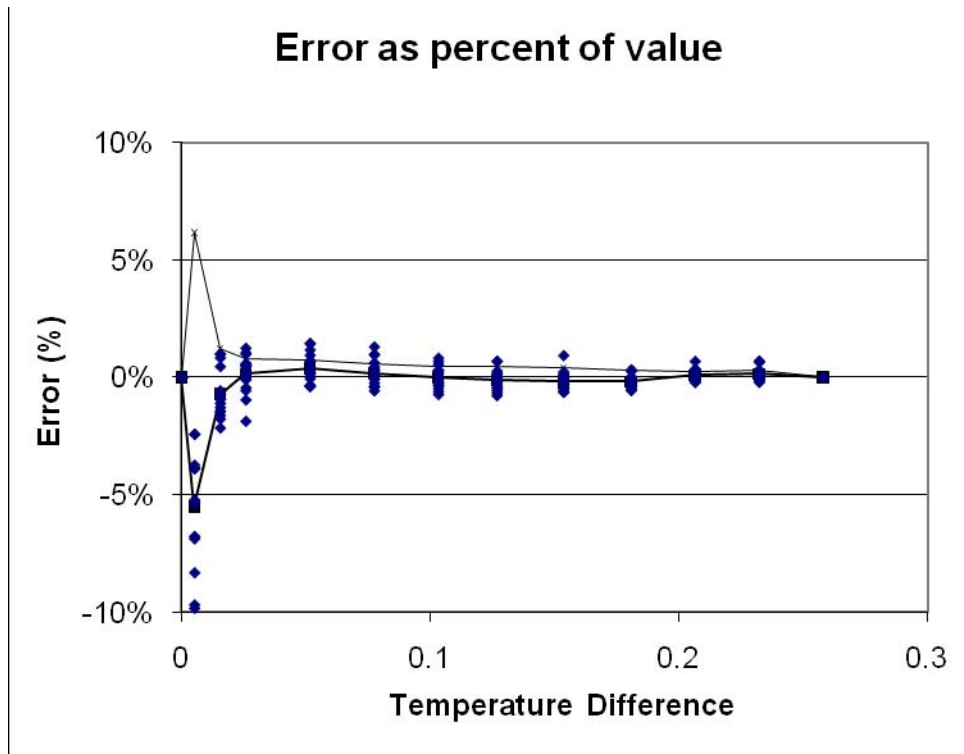


Figure 6. Error between universal curve and calibration points, as percent of the temperature difference. The mean error at any input temperature is shown as connected squares. Finally, the standard deviation of the calibration from the curve fit is shown as the line which remains in the positive portion of the graph.

## 5.2 Temperature Fluctuation

The thermosonde measures temperature fluctuations that are converted to optical turbulence levels.

### 5.2.1 Accuracy

During calibration, voltages are read within 1mV for a range of voltages from the minimum, which is the noise floor of about 10mV (equivalent to about 0.0005K) up to a maximum output of 2.0V<sup>11</sup>

## 5.2.2 Precision

With 1mV accuracy, the precision is two significant figures for noise floor voltage readings up to more than three significant figures at the highest output voltages.

## 5.2.3 Universal Calibration Curve

As shown above, the universal curve causes a small error, which has an uncertainty of about 6% at 0.005K, to well below a percent at values above 0.02K.

## 5.2.4 Noise Floor

The magnitude of the noise level of the current thermosonde has benefited from the aforementioned improvements. The noise level has decreased from an original level<sup>12</sup> equivalent to 0.004K, to approximately 0.002K in the 1980's<sup>13</sup>, to less than 0.001K today.

## 5.3 Effect of the Above Errors

Any calculation of  $C_n^2$  based on measured  $C_T^2$  is subject to uncertainties in the measured pressure, temperature, and temperature fluctuation. Assuming that these errors are uncorrelated with each other, standard uncertainty analysis<sup>13</sup> of the Equation (1-9) results in the following estimate of the error in  $C_n^2$ .

$$\left(\frac{\sigma_a}{C_n^2}\right)^2 = 4\left(\frac{\sigma_p}{P}\right)^2 + 16\left(\frac{\sigma_T}{T}\right)^2 + 4\left(\frac{\sigma_{\delta T}}{\delta T}\right)^2 \quad (17)$$

where  $\sigma_a$  is the total error and  $\sigma_p$ ,  $\sigma_T$ , and  $\sigma_{\delta T}$  are the uncertainties in pressure, temperature, and temperature fluctuation, the square root of  $C_T^2$ . The measured temperature differences vary from the noise floor to within a tenth of a degree. The pressure uncertainty factor can become important at the highest altitudes for high values of  $C_T^2$ . Temperature uncertainty is never significant. For the lowest values of  $C_T^2$ , the error is less than 10%, and decreases to well below a percent as  $C_T^2$  increases.

For a modest  $C_T^2$  value of  $0.0002 \text{ K}^2 \text{ m}^{-2/3}$ , the uncertainty in  $C_n^2$  is down to 1.5%. By a stronger  $C_T^2$  of 0.01, overall  $C_n^2$  uncertainty is below 0.5% at low altitudes, and starts to noticeably increase at 20km reaching a 4% uncertainty at 30km due to pressure uncertainties.

## **5.4 Other Instrument Related Factors:**

### **5.4.1 Heat Transfer – Altitude Limits**

As the thermosonde approaches the maximum altitude of 30km, the heat transfer coefficient has decreased to the point that the cutoff frequency of the instrument response approaches sizes that can impact the 1m-structure function. Therefore, altitudes higher than 30km are not recommended.

### **5.4.2 RMS Chip**

The proper computation of optical turbulence requires an accurate running root mean square of the temperature differences. In fact, commercially available RMS chips perform only an approximation to a true root mean square. The effective time constant of the calculation is not constant. When the temperature differences are short relative to the ~1s sampling period, which is associated with very low values of integrated turbulence, there can be an error of a factor of 2 in integrated optical turbulence. Numerical simulations with more typical distributions of simulated turbulence show errors of 10 to 20% in integrated turbulence<sup>8</sup>.

### **5.4.3 Telemetry system**

The output from the RMS chip is routed to an interface card with an accuracy of less than 2mV, which is well below the other errors mentioned in the report.

### **5.4.4 Environmental Factors**

Thermosondes normally ascend at approximately 5m/s from ground level to 30km attached to a large weather balloon by a 110m line. There are some inherent sources of uncertainty that must be considered: the wake of the balloon and inherent statistical issues in characterizing turbulence, with its random variations in space and time.

### **5.4.5 Balloon Wake**

The impact of the balloon wake is currently under investigation. A comparison of output from a normally ascending thermosonde to that of a downward facing thermosonde on a descending balloon showed that wake encounters have an insignificant effect in the troposphere, but can be significant in the stratosphere<sup>14</sup>. Encounters with a wake can occur in low shear environments<sup>15</sup> when measured values of atmospheric turbulence are usually low.

### **5.4.6 Stationarity – Homogeneity Issues**

Since the earliest thermosonde measurements (References 6, 7, and 13), there has been a concern about the ability to achieve an accurate mean value of the temperature fluctuations while ascending at around 5m/s. This is of particular concern when the layers are quite thin, since the instrument is only sampling the RMS chip at a frequency of about 1Hz. The turbulence layers that cause the most significant decrease in optical performance are usually thick enough that many samples are indicating nearly the same value. However, accurate measurement of thinner layers remains an unquantified source of uncertainty. A good statistical estimate of the mean requires sampling over several correlation lengths. The correlation length of the thermosonde measurement is roughly equivalent to the largest scales contributing to a 1 meter structure function and this is of the order of 10-20 meters. Hence, the intrinsic difficulty in obtaining good statistical estimation of  $C_n^2$  on an ascending balloon in layers less than 100 m thick is acknowledged.

## **6. Summary**

In summary, the thermosonde has the most uncertainty when measuring low values of turbulence. Near the noise floor, errors approach the size of the measurement. As the turbulence levels increase, uncertainties from all sources decrease to below 10% as the integrated turbulence levels approach that of Clear 1. The strongest levels of optical turbulence, which are the most important, reflect the region of highest accuracy of the instrument.

## REFERENCES

---

- <sup>1</sup> Regan, F.C., *Technical support for optical turbulence research*, AFGL-TR-88-0269, Air Force Geophysics Laboratory, Hanscom AFB, MA 01731, Aug 88.
- <sup>2</sup> Beland, R.R., *The Infrared and Electro-Optical System Handbook*, Vol. 2, *Atmospheric Propagation and Radiation*, edited by F.G. Smith, Infrared Information Analysis Center, Ann Arbor, MI, and SPIE Optical Engineering Press, Bellingham, WA, 1993, pp.157-232.
- <sup>3</sup> Kolmogorov, A.N., "The local structure of turbulence in incompressible viscous fluid for very large Reynolds numbers," *Dokl. Akad. Nauk SSSR*, Vol. 30, 4, 1941.
- <sup>4</sup> Corrsin, S., "On the spectrum of isotropic temperature fluctuations in isotropic turbulence." *J. Applied Physics*, Vol. 25, 657, 1951
- <sup>5</sup> Oboukhov, A.M., "Structure of the temperature field in turbulent flows," *Izvestiya Akademii Nauk SSR, Geogr. and Geophys. Ser.*, Vol. 13, 58, 1949.
- <sup>6</sup> Brown, J.H., R.E. Good, P.M. Bench, and G. Faucher, *Sonde Experiments for Comparative Measurements of Optical Turbulence*, AFGL-TR-82-0079, ADA 118 740, Air Force Geophysics Laboratory, Hanscom AFB, MA 01731, Feb 82.
- <sup>7</sup> Bufton, J.L., *A radiosonde thermal sensor technique for measurement of atmospheric turbulence*, NASA TN-D-7867, Goddard Space Flight Center, Greenbelt, MD 20771, Feb. 75.
- <sup>8</sup> Jumper, G.Y., R.R. Beland and P. Tracy, "Investigating Sources of error in balloon-borne optical turbulence measurements, AIAA 99-3618, 30<sup>th</sup> Plasmadynamics and Lasers Conference, June 99.
- <sup>9</sup> Advanced Continuous Simulation Language (ACSL), AEgis Research Corporation, Huntsville, AL.
- <sup>10</sup> Technical Information for RS80 Radiosondes, Vaisala Inc., 100 Commerce Way, Woburn, MA, USA
- <sup>11</sup> Technical Information for Fluke 87 Digital Volt Meter, PN 834192, Aug 88, Rev 6, 11/94, Fluke Corp., Everett, WA 98206.
- <sup>12</sup> Bufton, J. L cited above, p.7.
- <sup>13</sup> Brown, J.H. and R.R. Beland, "A Site Comparison of Optical Turbulence in the Lower Stratosphere at Night Using Thermosonde Data", *Physica Scripta.*, Vol. 37, pp. 424-426, 1988.
- <sup>14</sup> Jumper, G.Y. and E.A. Murphy, "Effect of Balloon Wake on Thermosonde Results", AIAA 2001-2796, 32<sup>nd</sup> AIAA Plasmadynamics and Lasers Conference, June 2001.
- <sup>15</sup> Barat, J., C. Cot and C. Sidi, "On the measurement of the turbulence dissipation rate from rising balloons", *Journal of Atmospheric and Oceanic Technology*, vol. 1, pp 270 – 275, Sep 1984.